Dynamic control of positional information in the early *Drosophila* embryo

Johannes Jaeger[1], Svetlana Surkova[2], Maxim Blagov[2], Hilde Janssens[1], David Kosman[3], Konstantin N. Kozlov[2], Manu[1], Ekaterina Myasnikova[2], Carlos E. Vanario-Alonso[1,4], Maria Samsonova[2], David H. Sharp[5] & John Reinitz[1]

[1]*Department of Applied Mathematics and Statistics, and Center for Developmental Genetics, Stony Brook University, Stony Brook, New York 11794-3600, USA*
[2]*Department of Computational Biology, Center for Advanced Studies, St Petersburg State Polytechnic University, St Petersburg, 195251 Russia*
[3]*Department of Biology, University of California, San Diego, California 92093, USA*
[4]*Universidade Federal do Rio de Janeiro, Instituto de Biofísica Carlos Chagas Filho, Rio de Janeiro, Rio de Janeiro 21949-900, Brazil*
[5]*Applied Physics Division, and Theoretical Division, Los Alamos National Laboratory, Los Alamos, New Mexico 87545, USA*

Morphogen gradients contribute to pattern formation by determining positional information in morphogenetic fields[1,2]. Interpretation of positional information is thought to rely on direct, concentration-threshold-dependent mechanisms for establishing multiple differential domains of target gene expression[1,3,4]. In *Drosophila*, maternal gradients establish the initial position of boundaries for zygotic gap gene expression, which in turn convey positional information to pair-rule and segment-polarity genes, the latter forming a segmental prepattern by the onset of gastrulation[5–7]. Here we report, on the basis of quantitative gene expression data, substantial anterior shifts in the position of gap domains after their initial establishment. Using a data-driven mathematical modelling approach[8–11], we show that these shifts are based on a regulatory mechanism that relies on asymmetric gap–gap cross-repression and does not require the diffusion of gap proteins. Our analysis implies that the threshold-dependent interpretation of maternal morphogen concentration is not sufficient to determine shifting gap domain boundary positions, and suggests that establishing and interpreting positional information are not independent processes in the *Drosophila* blastoderm.

The maternal Bicoid (Bcd) gradient in blastoderm-stage embryos of *Drosophila melanogaster* is a classic example of a morphogen gradient[12,13]. The modern morphogen concept[4] implies that Bcd by itself should be able to specify directly the domain boundaries of its target genes, such as the gap genes *Krüppel*(*Kr*), *giant*(*gt*) (Fig. 1a), *knirps*(*kni*) and *hunchback*(*hb*) (Fig. 1b). Genetic and theoretical studies suggest, however, that gap gene regulation by Bcd requires regulatory synergism with maternal Hb[9,14], and quantitative experiments show that Bcd by itself cannot account for the precise positioning of zygotic *hb* expression[12,15]. In addition, sharpening of gap domain boundaries and maintenance of gap gene expression rely on gap–gap cross-repression (see ref. 16, and references therein). It remains unclear, however, whether such cross-repression is required for correct positioning of gap gene boundaries, or if a combination of the maternal Bcd, Hb and Caudal (Cad) gradients is sufficient to determine positional information in the gap gene system.

Proof of the sufficiency of a given set of genetic interactions for specific expression patterns can be achieved only by reconstituting the underlying gene network from well-defined ingredients. Because this is currently impossible *in vitro*, we have used an *in silico* approach. The gene circuit method is a data-driven mathematical modelling approach for the computational reconstitution and

Box 1
The four steps of the gene circuit method

Step 1: Formulation of the model
Gene circuits are hybrid dynamical models consisting of discrete nuclear divisions and continuous intranuclear dynamics of protein concentrations. Nuclei indexed by i are arranged in a one-dimensional row along the A–P axis, because A–P and D–V patterning systems are largely independent in the trunk region of the embryo. Gap gene circuit models cover 58 nuclei between 35 and 92% A–P position during cycles 13 and 14A[27], and include *bcd*, *cad*, *hb*, *Kr*, *kni*, *gt* and the terminal gap gene *tll*. The rates of change in protein concentration dv_i^a/dt for each regulated gene product a in each nucleus i during interphase are given by a system of 348 ordinary differential equations defined by

$$\frac{dv_i^a}{dt} = R_a g(u^a) + D^a\left[(v_{i-1}^a - v_i^a) + (v_{i+1}^a - v_i^a)\right] - \lambda_a v_i^a \qquad (1)$$

The main terms on the right hand side of equation (1) represent protein synthesis, diffusion and decay respectively, with the corresponding rate parameters R_a, D^a and λ_a. Diffusion parameters are proportional to the inverse square distance between nuclei, which is halved on division. During mitosis, protein synthesis is shut down. Nuclear division occurs at the end of mitosis in cycle 13. $g(u^a)$ is a sigmoidal regulation–expression function, where u^a is given by

$$u^a = \sum_b T^{ab} v_i^b + m^a v_i^{\mathrm{Bcd}} + h^a \qquad (2)$$

For values of u^a below -1.5 and above $+1.5$, $g(u^a)$ rapidly approaches zero and one, respectively (broken lines in figure below).

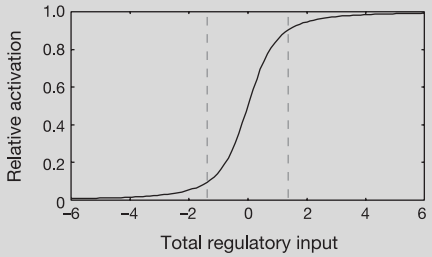

Parameters T^{ab} constitute a genetic interconnectivity matrix and represent activation of gene a by the product of gene b if positive, repression if negative, and no interaction if close to zero. v_i^{Bcd} represents the concentration of Bcd in nucleus i, which is exclusively maternal and constant in time. m^a describes the regulatory input of Bcd to the zygotic system. Maternal contributions to Hb and Cad are represented as nonzero initial conditions. h^a represents regulatory input from ubiquitous maternal factors (see Supplementary Information for details).

Step 2: Quantitative gene expression data
Quantified expression profiles for products of genes a at one time point in cycle 13 and eight time points during cycle 14A are used for fits of the model to data (see Methods).

Step 3: Optimization to fit model to data
Parameter values are not fixed *a priori*, but are obtained by fitting the model to data. Numerically calculated model output is compared with quantitative gene expression data, and the difference between the two is minimized by adjusting parameter values using the PLSA optimization method (see Methods). In this way, we obtain specific sets of parameters, and thus specific gene circuits, which faithfully reproduce the expression patterns used for optimization (see Supplementary Information for parameter values).

Step 4: Biological analysis
Regulatory parameters of gene circuits contain information about the generative mechanism underlying the expression data used for optimization. We extract this information by graphical analysis of both the reaction and diffusion terms of equation (1), and the quantitative regulatory contributions $T^{ab}v_i^b$ by regulators b to specific genes a in each nucleus i in equation (2).

analysis of observed gene expression patterns, which allows us to infer regulatory interactions from wild-type gene expression data[8–11,16] (Box 1).

Quantitative gene expression data show significant anterior shifts of gap domain boundaries during cleavage cycle 14A (Fig. 1c, e, g). Gap gene circuit models reproduce observed gap gene expression patterns, including boundary shifts of the central *Kr* domain and the posterior domains of *kni* and *gt*, with high precision and temporal resolution (Fig. 1d, f, h). Elsewhere, we have shown that our models also specifically and accurately reproduce the activation of gap genes by maternal factors and gap–gap cross-repression[16]. Taken together, this suggests that gap gene circuit models correctly represent the dynamic and genetic properties of the gap gene system.

In gap gene circuits, dynamic shifts of gap gene expression domains are reflected at the level of the rate of change in protein concentration (Fig. 2a–c). We can distinguish two discrete regulatory domains in the anterior and posterior portions of the *Kr*, *kni* and *gt* expression domains: protein synthesis dominates anteriorly, whereas protein decay posteriorly (Fig. 2d–f). The combination of anterior synthesis and posterior decay leads to an anterior shift of each expression domain. In addition, both the synthesis and decay domains themselves shift anteriorly over time (Fig. 2a–c).

The model thus predicts that synthesis is confined to the anterior region of each expression domain, implying that there is an asymmetric distribution of gap gene transcript in protein domains. Confirmation of this prediction is shown in Fig. 3. During cycle 14A, transcript domains of *Kr*, *kni* and *gt* are shifted anteriorly with respect to their corresponding protein domains (Fig. 3e–q). Such an asymmetrical distribution of *Kr* transcript and protein domains has been reported previously[17], but it has not been interpreted in terms of dynamical shifts. In addition, anterior shifts of domain boundaries are present at both the transcript and the protein level (Fig. 3), consistent with shifts in domains of synthesis, as observed in gene circuits (Fig. 2a–c).

A generative mechanism for gap domain shifts must explain the dynamic positioning of the domains of protein production and decay. Theoretically, shifts in domain boundaries can be caused by mechanisms based on gene regulatory interactions and/or the diffusion of gene products between neighbouring nuclei. In the syncytial blastoderm of *Drosophila*, the absence of cell membranes between nuclei allows the diffusion of gap gene products, leading to protein domains that, in general, are slightly larger than their corresponding transcript domains (Fig. 3).

Gene circuits allow us to examine the roles of regulatory and diffusive mechanisms by plotting the corresponding terms in the gene circuit equation (Box 1). Here, we illustrate our analysis with the example of the posterior boundary of *kni*. We compare temporal changes in protein concentration (Fig. 4a–c) to temporal changes in the reaction (protein synthesis and decay) and the diffusion terms of the equation (Fig. 4e–g). Nuclei that lie in the zone of the anterior shift of the posterior *kni* boundary show a characteristic switch from synthesis to decay of Kni protein during cycle 14A (Fig. 4a–c). This dynamical behaviour is directly responsible for the observed anterior shift of the boundary. It is closely mirrored by changes in the reaction terms of the equation, whereas diffusion leads to an influx of protein into the shift zone counteracting the boundary shift (Fig. 4e–g). For shifts in posterior borders, a counteracting role of diffusion is expected because the shift occurs toward increasing protein concentration in the boundary. But even for shifts in anterior boundaries, which occur in the direction of lower concentration, diffusion is not essential because these shifts are still present in gap gene circuits in which diffusion is not allowed to occur (see Supplementary Information). Thus, our analysis suggests that although gap protein diffusion is present in both embryo and gap gene circuits, it does not have a significant role in shifting gap domain boundaries.

Gene circuits allow us to study gene regulatory interactions by plotting combinations of regulatory contributions to the expression of a particular gene. For the shift in the posterior boundary of *kni*, we have found the following relevant regulatory contributions (Fig. 4i–k). Expression of *kni* is repressed in nuclei in the shift zone by spatially specific repressive inputs that counteract broad Cad activation throughout the posterior region of the embryo (Fig. 4i–k). Downregulation of *kni* in the posterior portion of the

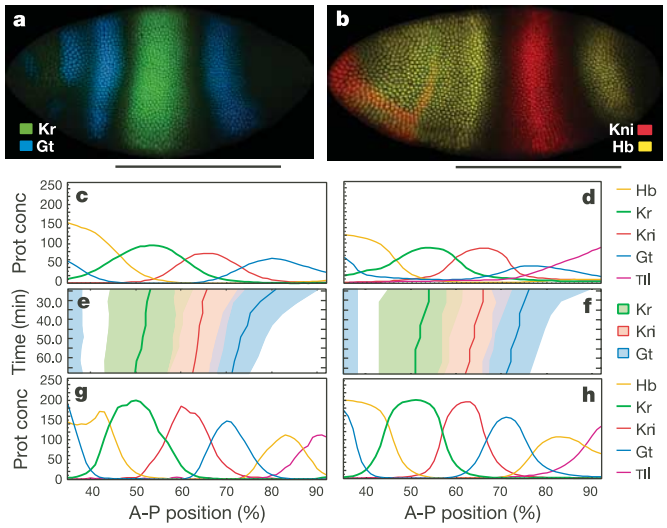

Figure 1 Dynamical shifts in gap gene domains are reproduced by gap gene circuits. **a**, **b**, *Drosophila melanogaster* blastoderm stage embryos at late cleavage cycle 14A (time class T8) immunostained for Kr and Gt (FlyEx embryo, rge9; **a**) and Kni and Hb (rb8; **b**). Anterior is to the left, dorsal is up. Bars indicate the region included in gap gene circuits. **c**, **d**, **g**, **h**, Gene expression data (**c**, **g**) and gap gene circuit model output (**d**, **h**) at early (T1; **c**, **d**) and late (T8; **g**, **h**) cycle 14A. Vertical axes represent relative protein concentrations, horizontal axes represent position along the A–P axis (where 0% is the anterior pole). There are no Tll data for T1 (**c**). **e**, **f**, Gap domain shifts for *Kr*, *kni* and *gt* covering the time between patterns shown in **c**, **d** and **g**, **h**. Lines indicate the position of maximum concentration for each domain. Coloured areas represent regions in which protein concentration is above the half-maximum value. Positional values for data were obtained by approximation with quadratic splines[22].

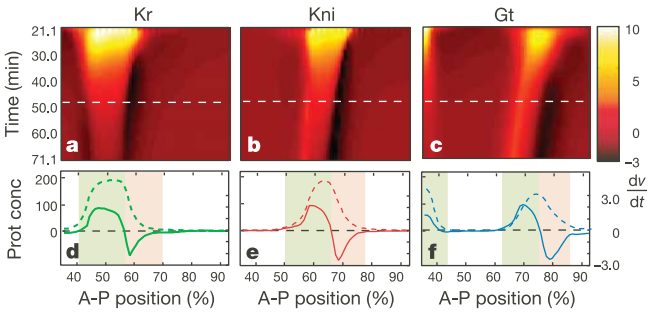

Figure 2 Shifting domains of gap protein synthesis and decay. **a**–**c**, Time–space diagrams, based on model output, of rate of change in protein concentration, d*v*/d*t*, for Kr (**a**), Kni (**b**) and Gt (**c**) during cycle 14A. Vertical axes represent time, horizontal axes represent position along the A–P axis. Note the shifting positions of domains of protein synthesis (yellow, light red) and protein decay (black). **d**–**f**, Cross-sections through **a**–**c** at time class T5 (broken white lines in **a**–**c**) for Kr (**d**), Kni (**e**) and Gt (**f**). Broken lines represent relative protein concentration, solid lines represent the rate of change in protein concentration, d*v*/d*t*. Domains of protein synthesis and decay are indicated by the light green and red backgrounds, respectively.

shift zone is caused by increasing repression by Gt (Fig. 4j), and *kni* is maintained in a repressed state throughout cycle 14A in more posterior nuclei owing to repression by Gt, Hb and Tailless (Tll; Fig. 4k). Expression of *gt* in the posterior portion of the *kni* domain (Fig. 4d, h), and hence increasing repression of *kni* by Gt (Fig. 4j), is made possible by an asymmetry in mutual regulatory interactions between *kni* and *gt*. *kni* is repressed by Gt, but there is no significant effect of Kni on *gt* (Fig. 4l). Note that the increasing repression of *kni* by Hb in the posterior portion of the shift zone is a consequence rather than a cause of the *kni* boundary shift (Fig. 4k). It occurs only in nuclei that do not express any *kni* because Kni is a very strong repressor of *hb* (Fig. 4c and Supplementary Information).

By contrast, more anterior nuclei show high levels of Kni synthesis in the absence of any significant repression (Fig. 4i). The

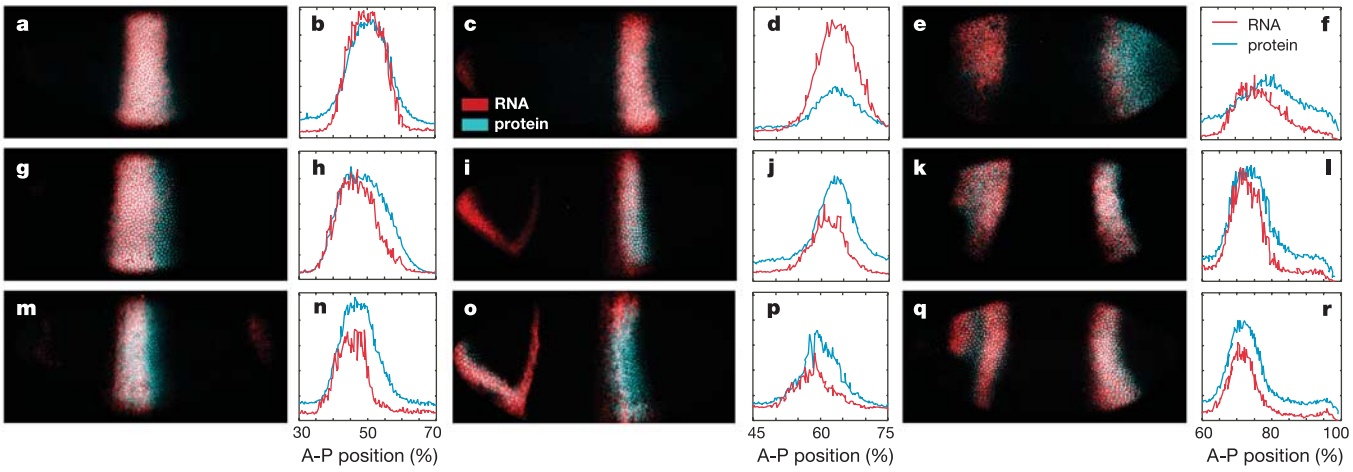

Figure 3 Gap domain boundary shifts as visualized by asymmetric distribution of transcript (RNA) and protein expression domains. Embryos fluorescently stained for RNA and protein products of *Kr* (**a**, **g**, **m**), *kni* (**c**, **i**, **o**) and *gt* (**e**, **k**, **q**), as well as the corresponding quantified expression graphs (*Kr*, **b**, **h**, **n**; *kni*, **d**, **j**, **p**; *gt*, **f**, **l**, **r**), are shown at early (**a**–**f**), mid (**g**–**l**) and late (**m**–**r**) cycle 14A. Vertical axes represent relative protein concentration, horizontal axes represent A–P position, as in Fig. 1c, d, g, h.

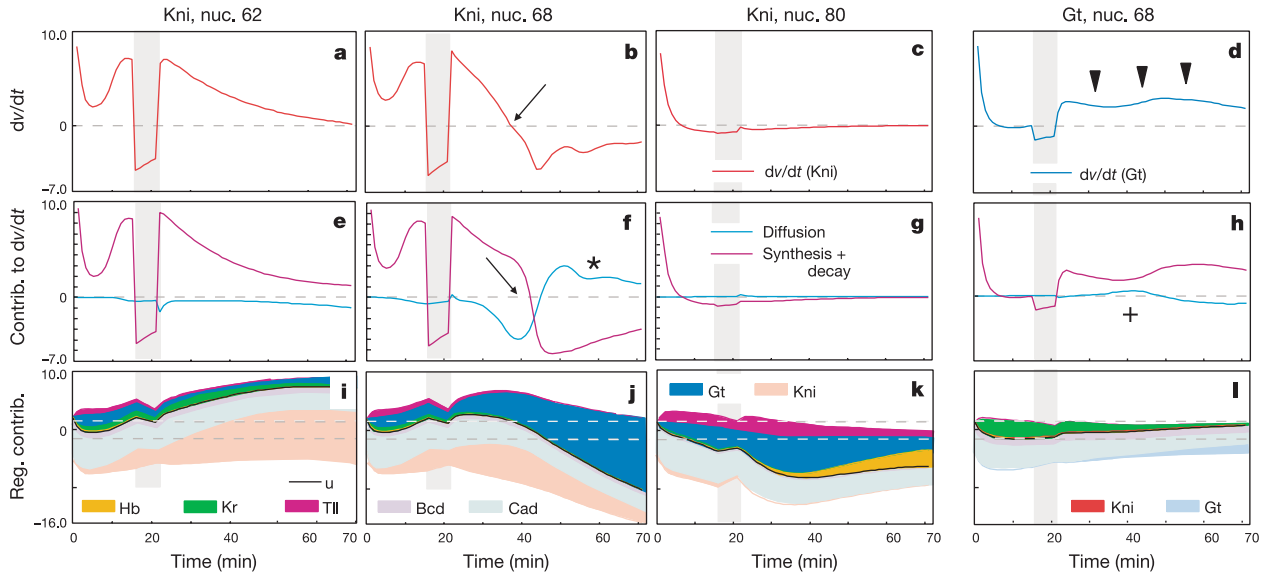

Figure 4 Graphical dynamic analysis of the regulatory mechanism for the shift in the posterior *kni* boundary. Regulatory graphs are shown for *kni* (**a**–**c**, **e**–**g**, **i**–**k**) and *gt* (**d**, **h**, **l**) over cycles 13 and 14A. **a**–**c**, **e**–**g**, Temporal behaviour of the rate of change in Kni protein production, d*v*/d*t* (**a**–**c**), and the diffusion, and the synthesis and decay terms of the gene circuit equation (**e**–**g**; see equation (1) in Box 1). Mitosis is shown as a shaded background. The zone of the shift in the posterior *kni* boundary is limited by an anterior nucleus (at 62% A–P position) that shows no Kni protein decay (**a**), and a posterior nucleus (at 80% A–P position) that shows no significant Kni protein synthesis at any time during cycle 14A (**c**). Nuclei in the zone (at 68% A–P position) show a switch from protein synthesis to decay during cycle 14A (arrow, **b**, **f**). Diffusion counteracts the boundary shift by generating an influx of protein into the zone of protein decay (asterisk, **f**). **d**, Gt synthesis in the nucleus at 68% A–P position is initiated at early cycle 14A and maintained at low levels throughout cycle 14A (arrowheads). **h**, Influx by diffusion contributes very slightly to the accumulation of Gt protein (plus). **i**–**l**, Temporal behaviour of regulatory contributions to *kni* (**i**–**k**) and *gt* (**l**) expression. Vertical axes show relative regulatory contribution. Positive values above the upper broken line represent protein synthesis at more than 90% of the maximum rate, negative values below the lower broken line represent repression, where protein synthesis is less than 10% of the maximum rate (Box 1). The sum of regulatory contributions, *u*, is represented by a black line. Coloured areas represent individual regulatory contributions by Hb, Kr, Gt, Kni, Tll, Bcd and Cad to *kni* (**i**–**k**) and *gt* (**l**). The height of each coloured area is given by $m^a v_i^{Bcd}$ for Bcd and by $T^{ab} v_i^b$ for all other regulators *b* (see equation (2) in Box 1).

increasing Kni synthesis in the anterior portion of the shift zone is largely caused by stably maintained Kni autoactivation (Fig. 4i). More posterior nuclei do not reach the threshold concentration of Kni required for stable maintenance of autoactivation and show only moderate transient (Fig. 4j) or no (Fig. 4k) Kni autoactivation. Localized autoactivation is a consequence of the asymmetric repressive mechanism described above, rather than a cause of shifting domain boundaries. This is corroborated by the fact that a gap gene circuit without *kni* autoactivation shows correct shifts of *kni* domain boundaries (see Supplementary Information).

We have also analysed shifts of other gap gene domain boundaries (see Supplementary Information). With the exception of the posterior boundaries of the anterior *hb* and *gt* domains, we have detected anterior shifts in all boundaries examined (Fig. 1c–h). The shifts of the posterior boundaries of *Kr* and posterior *gt* are caused by asymmetric repressive interactions between *Kr* and *kni*, and *gt* and *hb*, very similar to those described for *kni*. Posterior dominance of repressive interactions among neighbouring gap genes is reminiscent of homeotic gene regulation, where posterior homeotic genes repress more anterior ones, but not vice versa[18]. Shifts of anterior gap domain boundaries either follow the posterior boundary shifts of more anterior gap genes or are due to sharpening of the posterior boundaries of anterior *gt* and *hb*. For example, the upregulation of *gt* in nuclei anterior to its posterior expression domain follows diminished repression by Kr (Fig. 4l). Therefore, shifts of anterior gap domain boundaries can be considered to be secondary effects of the dynamic behaviour of posterior boundaries.

Our results indicate that maternal Bcd, Hb and Cad alone are not sufficient for positioning of gap gene domains and hence do not qualify as morphogens in a strict sense. As has been pointed out[19], an active role of target tissue in specifying positional information contradicts the traditional distinction between the instructive role of maternal morphogens and their passive interpretation[1]. The requirement of specific regulatory interactions in the target tissue for proper interpretation of positional information can be interpreted as a requirement for specific tissue competence[20]. In addition, the dynamical nature of positional information, as encoded by expression boundaries, suggests that positional information in the blastoderm embryo can no longer be seen as a static coordinate system imposed on the embryo by maternal morphogens[1]. Rather, it needs to be understood as the dynamic process underlying the positioning of expression domain boundaries, which is based on both external inputs by morphogens and tissue-internal feedback among target genes. □

Methods

Acquisition of quantitative data

Drosophila blastoderm embryos were immunostained for three segmentation gene products each[21]. Each embryo was stained for Even-skipped (Eve) protein for time classification and registration[22]. We scanned laterally oriented embryos by laser confocal microscopy. Scanned images were aligned along the anteroposterior (A–P) axis and segmented by using binary nuclear masks to yield per-nucleus expression data for each protein.

Processing of quantitative data

Embryos were classified temporally as belonging to cycles 12 (for initial conditions), 13, or eight equally distributed time classes (T1–T8) in cycle 14A. Temporal classification in cycle 14A is based on the highly dynamic expression pattern of *eve*[22]. Expression patterns were registered by using a fast dyadic wavelet transform[22]. We removed nonspecific background staining. Data from the middle 10% of dorsoventral (D–V) positional values of each embryo were averaged for each gene and time class to yield an integrated data set that currently contains data based on 954 embryos, available in the FlyEx Database (http://urchin.spbcas.ru/flyex).

RNA/protein double staining

RNA was detected using digoxigenin-labelled RNA probes[23]. RNA hybridization was done before protein detection by using standard protocols with the exception of permeabilization, where Proteinase K was replaced by acetone treatment[24]. We obtained quantified expression profiles by image segmentation as described above.

Numerical simulations

Simulator and optimizer code was implemented in C, Java and Perl and is available on the Reinitz Lab website (http://flyex.ams.sunysb.edu/lab/gaps.html). Ordinary differential equations were solved numerically by using a Bulirsch–Stoer adaptive step size method[25]. Integration was done to 0.1% accuracy, and the stability of solutions was confirmed.

Optimization

The sum of squared differences between model and data was minimized using parallel Lam simulated annealing (PLSA)[10,26]. Search spaces were defined by explicit limits as well as a penalty function[10]. Each optimization run was done in parallel on ten 2.4-GHz Pentium P4 Xeon processors and took between 8 and 160 h per gene circuit.

Gene circuit selection and analysis

Because PLSA is a stochastic method, the quality of the resulting gene circuits can vary. Best solutions were selected as described elsewhere[16]. The selection process yielded 10 circuits (out of 40), which were used in the present analysis (see Supplementary Information). These circuits show strong constraints toward a specific gap gene network topology[16]. All data shown here are based on one particular gap gene circuit that shows no visible patterning defects and corresponds exactly to the network topology observed in most selected circuits.

Received 12 April; accepted 20 May 2004; doi:10.1038/nature02678.

1. Wolpert, L. Positional information and the spatial pattern of cellular differentiation. *J. Theor. Biol.* **25,** 1–47 (1969).
2. Crick, F. Diffusion in embryogenesis. *Nature* **225,** 420–422 (1970).
3. Lewis, J., Slack, J. M. W. & Wolpert, L. Thresholds in development. *J. Theor. Biol.* **65,** 579–590 (1977).
4. Gurdon, J. B. & Bourillot, P. Y. Morphogen gradient interpretation. *Nature* **413,** 797–803 (2001).
5. Nüsslein-Volhard, C. & Wieschaus, E. Mutations affecting segment number and polarity in Drosophila. *Nature* **287,** 795–801 (1980).
6. Akam, M. The molecular basis for metameric pattern in the *Drosophila* embryo. *Development* **101,** 1–22 (1987).
7. Ingham, P. W. The molecular genetics of embryonic pattern formation in *Drosophila*. *Nature* **335,** 25–34 (1988).
8. Mjolsness, E., Sharp, D. H. & Reinitz, J. A connectionist model of development. *J. Theor. Biol.* **152,** 429–453 (1991).
9. Reinitz, J., Mjolsness, E. & Sharp, D. H. Cooperative control of positional information in *Drosophila* by *bicoid* and maternal *hunchback*. *J. Exp. Zool.* **271,** 47–56 (1995).
10. Reinitz, J. & Sharp, D. H. Mechanism of *eve* stripe formation. *Mech. Dev.* **49,** 133–158 (1995).
11. Reinitz, J., Kosman, D., Vanario-Alonso, C. E. & Sharp, D. H. Stripe forming architecture of the gap gene system. *Dev. Gen.* **23,** 11–27 (1998).
12. Driever, W. & Nüsslein-Volhard, C. The Bicoid protein determines position in the *Drosophila* embryo in a concentration-dependent manner. *Cell* **54,** 95–104 (1988).
13. Ephrussi, A. & St Johnston, D. Seeing is believing: the Bicoid morphogen gradient matures. *Cell* **116,** 143–152 (2004).
14. Simpson-Brose, M., Treisman, J. & Desplan, C. Synergy between the Hunchback and Bicoid morphogens is required for anterior patterning in *Drosophila*. *Cell* **78,** 855–865 (1994).
15. Houchmandzadeh, B., Wieschaus, E. & Leibler, S. Establishment of developmental precision and proportions in the early *Drosophila* embryo. *Nature* **415,** 798–802 (2002).
16. Jaeger, J. *et al.* Dynamical analysis of regulatory interactions in the gap gene system of *Drosophila melanogaster*. *Genetics* (in the press).
17. Gaul, U., Seifert, E., Schuh, R. & Jäckle, H. Analysis of Krüppel protein distribution during early *Drosophila* development reveals posttranscriptional regulation. *Cell* **50,** 639–647 (1987).
18. McGinnis, W. & Krumlauf, R. Homeobox genes and axial patterning. *Cell* **68,** 283–302 (1992).
19. Meinhardt, H. Space-dependent cell determination under the control of a morphogen gradient. *J. Theor. Biol.* **74,** 307–321 (1978).
20. Waddington, C. H. *Organisers and Genes* (Cambridge Univ. Press, Cambridge, UK, 1940).
21. Kosman, D., Small, S. & Reinitz, J. Rapid preparation of a panel of polyclonal antibodies to *Drosophila* segmentation proteins. *Dev. Genes Evol.* **208,** 290–294 (1998).
22. Myasnikova, E., Samsonova, A., Kozlov, K., Samsonova, M. & Reinitz, J. Registration of the expression patterns of *Drosophila* segmentation genes by two independent methods. *Bioinformatics* **17,** 3–12 (2001).
23. Tsai, C. & Gergen, J. P. Gap gene properties of the pair-rule gene *runt* during *Drosophila* segmentation. *Development* **120,** 1671–1683 (1994).
24. Nagaso, H., Murata, T., Day, N. & Yokoyama, K. K. Simultaneous detection of RNA and protein by *in situ* hybridization and immunological staining. *J. Histochem. Cytochem.* **49,** 1177–1182 (2001).
25. Press, W. H., Teukolsky, S. A., Vetterling, W. T. & Flannery, B. P. *Numerical Recipes in C* (Cambridge Univ. Press, Cambridge, UK, 1992).
26. Chu, K. W., Deng, Y. & Reinitz, J. Parallel simulated annealing by mixing of states. *J. Comp. Phys.* **148,** 646–662 (1999).
27. Foe, V. E. & Alberts, B. M. Studies of nuclear and cytoplasmic behaviour during the five mitotic cycles that precede gastrulation in *Drosophila*. *J. Cell Sci.* **61,** 31–70 (1983).

Supplementary Information accompanies the paper on **www.nature.com/nature**.

Acknowledgements We thank J. P. Gergen for the constructs for RNA probes; and N. Monk, J. Dallman, J. D. Baker and L. Carey for comments on the manuscript. This work was supported financially by the NIH.

Competing interests statement The authors declare that they have no competing financial interests.

Correspondence and requests for materials should be addressed to J.R. (reinitz@odd.bio.sunysb.edu).